AIAA JOURNAL
Vol. 45, No. 4, April 2007

Dual-Pump Coherent Anti-Stokes Raman Scattering Measurements in a Supersonic Combustor

S. O'Byrne*
University of New South Wales, Australian Defence Force Academy, Canberra, Australian Capital Territory 2600, Australia
P. M. Danehy† and S. A. Tedder‡
NASA Langley Research Center, Hampton, Virginia 23681
and
A. D. Cutler§
George Washington University, Newport News, Virginia 23602

DOI: 10.2514/1.26768

The dual-pump coherent anti-Stokes Raman scattering (CARS) method was used to measure temperature and the mole fractions of N_2 and O_2 in a supersonic combustor. Experiments were conducted in NASA Langley Research Center's Direct-Connect Supersonic Combustion Test Facility. In this facility, H_2- and oxygen-enriched air burn to increase the enthalpy of the simulated air test gas. This gas is expanded through a Mach 2 nozzle and into a combustor model consisting of a short constant-area section followed by a small rearward-facing step and another constant-area section. At the end of this straight section, H_2 fuel is injected at Mach 2 and at a 30-deg angle with respect to the freestream. One wall of the duct then expands at a 3-deg angle for over 1 m. The ensuing combustion is probed optically through ports in the side of the combustor. Dual-pump CARS measurements were performed at the facility nozzle exit and at four planes downstream of fuel injection. Maps are presented of the mean temperature, as well as N_2 and O_2 mean mole-fraction fields. Correlations between fluctuations of the different measured parameters are also presented.

Introduction

SUPERSONIC combustion involves a complex interaction between turbulent mixing and chemical reaction. Whether efficient supersonic combustion occurs depends strongly upon the rate and extent to which chemical reactions occur compared to the residence time of the fluid in the combustor. In addition, no current ground testing facility is capable of perfectly reproducing the conditions of a real combustor in flight, due to the excess water (and often also carbon dioxide) in combustion-vitiated facilities, and the vibrational nonequilibrium, excess nitric oxide and atomic species, and short test times of pulsed facilities. If all these effects are to be accounted for, it is important to have available nonintrusive and spatially resolved methods for determining the location and extent of chemical reaction within an engine.

Modeling fuel–air mixing and combustion using computational fluid dynamics (CFD) requires quantitative data from within the flow to evaluate the performance of turbulent mixing models and to develop new models. Although measurements of surface properties such as pressure and heat transfer are commonplace, quantitative or semiquantitative measurements of flowfield properties are difficult to obtain, and hence there are far fewer examples in the literature. Nonintrusive measurements have been performed in supersonic mixing and combustion experiments using coherent anti-Stokes Raman scattering (CARS) [1–7], laser-induced fluorescence (LIF) [8–11], and other techniques. Whereas CARS can obtain pointwise multiparameter measurement of flow properties for major species such as N_2 and O_2, LIF provides spatially resolved flowfield visualization and measurements of temperature and mole fraction for minority species. Information about OH, CH, and other radical species provided by LIF is particularly useful in understanding combustion interactions. LIF is also easily extended to planar measurements, allowing instantaneous and high-spatial-resolution data to be acquired. However, LIF has not been used to produce quantitative measurements of mole fraction for majority species such as H_2, N_2, and O_2 in combusting flow. Thus, CARS and LIF are complementary measurement techniques.

Some forms of the CARS technique [12] are particularly valuable in performing quantitative studies of supersonic combusting flows because they have the potential to measure temperature and the concentrations of multiple important combustion species simultaneously. Other techniques such as Raman scattering can measure the same quantities, but CARS has the advantage of producing a coherent signal beam. This increases the signal-to-background ratio of measurements and permits spatial filtering to reduce the degradation of measurement quality due to interference from flow luminosity. The coherent nature of the CARS signal also means that good signal-to-noise ratio measurements can be made where optical access to the flow is limited, which is typically the case for scramjet combustors. When flow properties are measured simultaneously, correlations between the different species mole fractions and between the temperature and species mole fractions can be measured. These correlations can then be used to evaluate parameters in proposed turbulence models in Reynolds-averaged Navier–Stokes codes, or to determine the effectiveness of large eddy simulation turbulence models.

There are several varieties of the CARS technique, and the choice of a particular method has a significant effect upon the difficulty and results of a given supersonic combustion experiment. Broadband N_2 vibrational CARS is one of the most commonly used variants and has proved very useful for providing temperature measurements in a number of supersonic combustion studies [1,2,6,7], but it is difficult to make mole-fraction measurements [12]. Because mole fractions of

Presented as Paper 710 at the 42nd AIAA Aerospace Sciences Meeting and Exhibit, Reno, NV, 5–8 January 2004; received 25 July 2006; accepted for publication 19 December 2006.

*Postdoctoral Fellow; formerly NRC Postdoctoral Fellow at NASA Langley Research Center. Member AIAA.
†Research Scientist. Associate Fellow AIAA.
‡Graduate Co-Op Student; currently Graduate Student, College of William and Mary, Williamsburg, VA 23187-8795.
§Professor. Associate Fellow AIAA.

the species other than N_2 are not generally known, their contribution to nonresonant susceptibility will also not be known, and this quantity is required for an absolute measurement of mole fraction.

To obtain more information about composition of the combusting flow, various multispecies techniques have been developed. The three most used methods are dual-Stokes CARS, pure-rotational CARS, and dual-pump CARS [12]. Dual-Stokes CARS, in which two broadband beams interact with two pump beams to produce two spatially and spectrally separated CARS signals simultaneously, has been used for multispecies measurements [5,13,14]. This system requires accurate measurement of all three laser intensities and calibration of multiple detectors to make quantitative measurements of mole fractions. Pure-rotational CARS [15,16] is another variation that measures multiple species. The pure-rotational CARS spectra for all species occur in the same spectral region, which is very useful for multispecies measurements, although for the same reasons pure-rotational spectra can become very complex, making it difficult to separate spectral contributions from different species. In general, rotational CARS is more sensitive at low temperatures, but vibrational CARS spectra are more sensitive to temperature variations at flame temperatures [17].

In this paper, we use the dual-pump CARS method developed by Lucht [18] and Hancock et al. [19] and extended by us, to simultaneously measure temperature and the absolute mole fractions of N_2 and O_2 in a supersonic combustion experiment. This experiment followed on from an initial experiment at the same nominal conditions in which conventional broadband N_2 CARS was used to map the temperature field in a supersonic combustor [1]. Using dual-pump CARS in the current experiment allowed the temperature field and species mole-fraction fields to be simultaneously measured. Like pure-rotational CARS, dual-pump CARS allows the signals from multiple species to appear in the same spectral region so that they can be captured on a single detector. Because the same three beams are used in the excitation process for all species, relative beam energies need not be measured, nor do multiple detectors need to be calibrated. Unlike pure-rotational CARS, dual-pump N_2–O_2 CARS provides some flexibility in the spectral location of the O_2 signal relative to the N_2 signal, minimizing overlaps between the spectra. Furthermore, the relative intensity of the O_2 and N_2 CARS signals is unaffected by beam steering, an important consideration in supersonic combustion flows. This supersonic combustion experiment is complemented by an analogous nonreacting case in which the same dual-pump CARS system has been used to study fuel–air mixing at the same nominal freestream conditions [20].

Conventional broadband N_2 CARS uses two spectrally narrow green beams as pump beams and one spectrally broad red beam as the Stokes beam. The frequency difference between the green and red beams typically corresponds to the vibrational Raman shift of N_2. The CARS signal is then a faint, spectrally broad blue beam that contains the N_2 spectrum. This spectrum can be detected and then fitted with a theoretical model on a computer to determine the temperature. The dual-pump CARS technique used here differs from the conventional broadband N_2 CARS technique because it uses two different colors for the pump beams: one green and the other yellow. The same broadband red beam is used as in conventional broadband N_2 CARS. The frequency of the yellow pump beam is chosen so that the frequency difference between the yellow and red beams excites the vibrational Raman transitions of O_2, with the green and red beams exciting the vibrational Raman transitions of N_2. The resulting blue CARS spectrum contains both N_2 and O_2 spectra. The relative intensities of these two spectra provide a measure of the relative mole fractions of N_2 and O_2.

Coincidentally, several pure-rotational Raman transitions of H_2 are present in these spectral regions as well, as described in [20,21]. These H_2 transitions were measured in the present experiment, in principle allowing the relative mole fractions of N_2, O_2, and H_2 to be quantified simultaneously. However, comparisons between calculations and measurements of H_2 mole fraction in an atmospheric pressure flame showed that the measured H_2 mole fraction was too low by 10–15% compared to the predictions from an adiabatic flame calculation, perhaps owing to errors in our spectral lineshape modeling. Thus, the H_2 measurements have been excluded from the current paper. Recently, other studies have also simultaneously measured N_2, O_2, and H_2 in a flame, using triple-pump CARS [22], but the system described here has the advantage of requiring one fewer laser and therefore being simpler to implement. In this paper we also demonstrate that applying N_2–O_2–H_2 dual-pump CARS to H_2–air combustion has an important advantage: simultaneous measurement of CARS signal from three out of the four major species provides sufficient information about the gas composition, and hence the contributions of the major species to the nonresonant susceptibility, to allow absolute N_2 and O_2 mole fractions to be determined. During previous use, dual-pump CARS has only allowed determination of ratios of species mole fractions, such as CO_2/N_2 ratio [23].

Combustor Model and Flow Facility

The experimental facility, model, and operating conditions are nominally identical to those tests described in [1], although the present tests were conducted some two years after. Many of the method descriptions herein are similar to those of [1], but have been repeated for convenience.

The experiment was conducted in NASA Langley's Direct-Connect Supersonic Combustion Test Facility (DCSCTF). The facility is designed to test the combustor of a scramjet engine by directly connecting the facility nozzle exit to the entrance of the combustor. The stagnation enthalpy of the gas is increased by burning H_2 in air and replenishing the O_2 lost in the combustion. The nozzle gas flow rates are selected so that the mass fraction of O_2 is the same as that of standard air. This high-pressure, vitiated gas is accelerated through a water-cooled convergent–divergent Mach 2 nozzle, before entering the test model.

The nominal test conditions are nearly identical to those presented in a previous single-pump CARS study [1], and are representative of Mach 7 flight. Gas flow rates to the heater are: 0.916 ± 0.008 kg/s air, 0.0284 ± 0.0006 kg/s H_2, and 0.302 ± 0.005 kg/s O_2. The heater stagnation pressure is 0.765 ± 0.008 MPa. All uncertainties presented in this paper are based on the 95% confidence interval half widths ($CIHW_{95\%}$), equivalent to 1.96 times the standard deviation divided by the square root of the number of samples. These uncertainties are due to the random run-to-run variations and do not include $\pm 3\%$ uncertainty in the mass flow rate measurements.

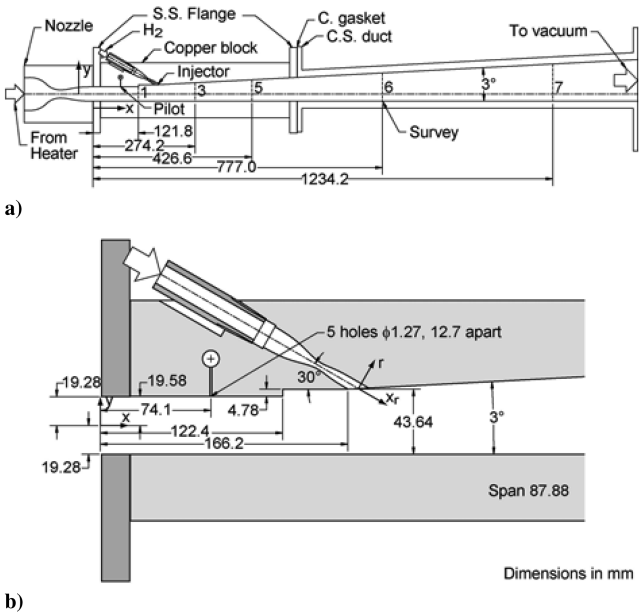

Fig. 1 a) Schematic of scramjet combustor model. b) Close-up of injection region. (From Cutler et al. [1].)

Heater and nozzle exit conditions were estimated in [1] from the flow rates, heater pressure, and nozzle minimum and exit areas using 1-D analysis detailed in [24] and assuming equilibrium chemistry. The nominal calculated conditions and uncertainties due to mass flow rate measurement error and run-to-run variations in heater conditions are as follows: heater stagnation temperature 1818 ± 75 K, exit static temperature 1181 ± 60 K, mole fraction O_2 0.186, mole fraction N_2 0.512, exit static pressure 100 ± 1.5 kPa, and exit Mach number 1.989 ± 0.005. Errors arising from the assumption of 1-D flow (the effects of nonuniform composition, boundary layers, etc.) are assumed to be small. A study of the flow quality at the exit of the facility nozzle was previously conducted and is described in [25].

The test model, known as the Scholar model, is shown in Fig. 1; flow direction is from left to right. The model consists of two main duct sections: a copper upstream section and a carbon steel downstream section. Stainless steel flanges and carbon gaskets separate the sections from each other and from the nozzle. Proceeding from left to right, there is a Mach 2 nozzle, a constant-area segment, a small outward step at the top wall, a second short constant-area segment and a segment with constant 3-deg divergence of the top wall. The span is constant at 87.88 mm. The fuel injector is located immediately downstream of the start of the 3-deg divergence. The injection angle is 30 deg to the opposite wall. The injector nozzle is designed by the method of characteristics to produce Mach 2.5, 1-D flow at the injector exit. Hydrogen is injected at a stagnation pressure of 3.44 ± 0.065 MPa[¶] and a stagnation temperature of 302 ± 4 K. This fuel flow rate corresponds to an overall equivalence ratio of 0.99 ± 0.04 for the gas in the duct.

The duct is not actively cooled; however, the wall thickness of the copper duct is greater than 32 mm and the carbon steel duct is 19 mm thick. Thus, given the good thermal conductivity of these materials, it is possible to operate the facility with the model fueled for run times in excess of 20 s without reaching excessive temperatures. With atmospheric-temperature air flowing in the model between runs, the tests can be repeated every 10 to 15 min. A total of 15–25 runs could be obtained per day.

The model is equipped with seven pairs of slots, to allow the CARS beams to enter and exit the duct. The first slot is at the nozzle exit and the other six slots are downstream of the fuel injection, as shown in Fig. 1. Slots 1, 3, 5, 6, and 7 were used in this study. The slots are used in pairs, one on each side of the duct. They are 4.8 mm wide and extend the full height of the duct. When not in use, the slots are plugged flush to the duct wall. Windows covering the slots are mounted at the end of short rectangular tubes at the Brewster angle, to minimize reflections. The tubes connecting the windows and combustor are ventilated with a constant flow of electrically heated ($\sim$400 K) dry air to prevent condensation of water vapor from the facility on the windows. The CARS interaction region (the measurement volume) can be translated the full span and height of the duct without damaging the windows. The supersonic combustor model is also instrumented with pressure taps and wall temperature probes, and measurements using these probes have been presented previously for the same configuration and flow conditions as the present experiment [1].

CARS Experimental System

A complete description of the dual-pump CARS system is given in [26]. It used an unseeded frequency-doubled Nd:YAG laser (Spectra Physics DCR-4), producing about 550 mJ per pulse at 532 nm with $\sim$1 cm^{-1} line width. The pulse duration was 10 ns and the repetition rate was 10 Hz. The output of the YAG laser was split three ways. Approximately 80 mJ was used as the green pump beam for CARS. A custom-built, axially pumped broadband dye laser operating at 607 nm was pumped using 250 mJ of green light from the doubled Nd:YAG. The dye solution consisted of rhodamine 640 laser dye in methanol, and the dye laser energy immediately before entering the periscope and focusing lens arrangement was 20–25 mJ.

Another 200 mJ of 532-nm light was used to pump a yellow (554-nm) narrowband dye laser (Lambda Physik, FL3002, which was modified according to the manufacturer's instructions from excimer to YAG pumping), producing 25 mJ of yellow light. The green and red beams were combined using a dichroic mirror. These two beams and the yellow beam were then passed through a spherical lens having a focal length of 410 mm. The planar BoxCARS phase-matching geometry was used [12], with the green and red beams overlapping. The probing volume formed at the intersection of the three beams had a minimum diameter of 130 μm, full width at half maximum (FWHM), measured by traversing a knife edge across the foci of all three beams and measuring unblocked light. The probe volume was 1.8 mm long (FWHM), measured by traversing the probe volume across a thin planar jet of N_2 gas, surrounded by a 30-mm-diam jet of argon, and measuring the N_2 CARS signal as the probing volume was traversed across the N_2 sheet.

A second 410-mm focal-length lens collected and collimated the three input beams and the 491-nm CARS signal beam. Two dichroic mirrors, efficiently reflecting blue light while transmitting yellow and green light, were arranged in a multireflection configuration to isolate the blue signal beam. This blue beam was then directed into a 1-m focal-length spectrometer (McPherson) with a 1200-groove/mm grating. Two cylindrical lenses provided a sharp horizontal focus at the spectrometer entrance that was imaged, spectrally dispersed, at the detector. The detector was an 1100×330-pixel, nonintensified, back-illuminated CCD camera (Pixel Vision, SV11CBJ). A LabVIEW interface downloaded the spectra to a PC for subsequent analysis and could display spectra in real time for signal optimization. The 330-pixel region was binned into three separate rows of 110 pixels before being read out, to allow more rapid acquisition of data. This resulted in three 1100-pixel spectra per laser pulse, with a spectral resolution of 0.74 cm^{-1} per pixel. The pixel resolution is not the limiting factor for the spectral resolution of the CARS signal: the instrument function of the spectrometer–camera system was measured using best fits to CARS spectra obtained in room-temperature air, having an average FWHM of 1.5 cm^{-1}. The spectral width of the Nd:YAG pump laser is approximately 1 cm^{-1}.

The CARS signal was imaged onto the first two of the three binning regions, with the contributions of dark noise and laser scatter acquired on the third bin region. Distributing the signal over two bin regions increased the dynamic range of the measurements by up to a factor of 2. The binned background was subtracted from each of the signal bin regions before the signal regions were summed to form the total spectrum.

The spectral nonuniformity of the broadband Stokes laser was accounted for by normalizing the CARS spectrum to the "nonresonant" CARS spectrum obtained immediately after completion of the day's runs. The nonresonant CARS spectrum, which varies with the profile of the broadband laser, was measured by obtaining a CARS spectrum in a flow of argon (which has no resonances in this range of wavelength), averaged over 200 laser pulses. The spectral shape of the broadband laser envelope was well represented by the sum of two Gaussian functions. The higher amplitude of the two Gaussians fitted the majority of the broadband laser profile, whereas a wider, lower-amplitude Gaussian was necessary to ensure proper modeling of the wings of the broadband laser spectrum. Correctly fitting the broadband laser profile near the wings is important because the CARS spectrum can include strong H_2 lines near the edge of the profile. The peak frequencies of the two summed Gaussian functions were free to vary independently of each other, but the symmetry of the broadband laser profile ensured that the center frequencies of the two fitted Gaussians were very similar. The full width at half maximum of the nonresonant spectrum was approximately 130 cm^{-1} in the spectral region of the CARS signal imaged by the camera. This was sufficiently broad to contain spectral features of all three species of interest. The fitted function was used for the normalization of all spectra in a given experimental run.

[¶]In [1], the stagnation pressure of primary injected H_2 was incorrectly reported as 2.12 MPa.

CARS Spectral Data Analysis

The analysis of the CARS spectra differs in several important ways from the analysis reported in our previous paper [1], due to both the wider spectral region being fitted and to the larger number of fit parameters. The most important changes will now be discussed.

The broadband Stokes laser spectrum varies during a day's facility runs by as much as 30 cm^{-1}, due to alignment and temperature fluctuations in the optical system. Because important spectral features occur in the wings of the nonresonant spectrum where normalization causes signal levels to be particularly sensitive to changes in the spectral location of the Stokes beam, the analysis must account for these changes. This was done by allowing the nonresonant CARS spectrum to shift in wavelength, while maintaining spectral width and shape, as part of the fitting process. For each tunnel run, the middle one third of acquisitions was fitted for temperature and the mole fractions of the three species using the nonresonant spectrum acquired in argon gas before the day's facility runs. The same spectra were then fitted twice more using the same nonresonant spectrum shifted by 7.4 cm^{-1} above and below the nominal spectral location. A systematic spectral offset in the center of the Stokes spectrum manifests as a gradient in the nonresonant CARS signal. The most correct of the Stokes spectra produces the smallest residual in the fitted spectra. If the middle of the three Stokes spectra used for normalizing the tunnel CARS spectra did not have the minimum residual, the center of the Stokes beam spectrum would be shifted another 7.4 cm^{-1} in the direction of decreasing residual until a minimum was found. A parabola was fitted to the residual at these three lowest-residual points and the minimum of that parabola was used as the location of the center of the Stokes beam spectrum for all the fits in that facility run. This procedure was repeated for all the facility runs on each day, and determined the shift in the Stokes laser spectrum to within 3.5 cm^{-1}, or 2.7% of the Stokes laser's FWHM. The noise in the residual prevented the Stokes laser shift being determined more accurately than this.

Individually measured CARS transitions are spectrally broader than theoretical transitions, mainly due to the low-resolution dispersion of the spectrometer. The shape and width of this broadening, known as the "instrument function," was determined by fitting room-temperature air spectra on each day tunnel data were acquired. The width and amplitude of the instrument function were varied using a nonlinear least-squares algorithm to produce the best fit for the known room-temperature air parameters. This fitted instrument function was used to generate the library of theoretical spectra for that day's runs. A version of the CARSFIT code [27], originally developed at Sandia National Laboratories, Livermore, CA, and modified for the dual-pump CARS technique by Hancock et al. [19], was used to compute the theoretical CARS spectra.

In our previous paper [1], temperature and N_2 mole fraction were fitted for each measured CARS spectrum by computing spectra at a large number of discrete temperature and mole-fraction values. Once this database of spectra had been calculated, the least-squares best fit was determined by comparison with the measured spectrum. The measurements in this paper could not be fit with the same resolution, because there were two additional fit parameters, the mole fractions of O_2 and H_2, and because the fitting of the very narrow H_2 transitions required higher spectral resolution in the library. To quickly fit the many thousands of CARS spectra obtained in the experiment, CARSFIT was used to generate a coarse 4-D (temperature, N_2, O_2, and H_2 mole fractions) library of spectra, using the Voigt profile to model the individual Raman transition lineshapes and assuming that the only other gas present was H_2O. No attempt was made to account for the concentrations of minor species such as the hydroxyl radical, nitric oxide, or argon. We modified the CARSFIT code to include convolutions with a second pump beam [20], as the previous version of the code assumed one of the pump beams to be monochromatic. The Nd:YAG laser used in these experiments was not injection-seeded, so the laser line width is large compared to the line width of the individual Raman transitions. We also removed from the code an error in the adaptive grid calculation, allowing the faster adaptive grid calculation to be used for H_2 spectrum calculations.

The measured N_2, O_2, and H_2 mole fractions were used to estimate the nonresonant susceptibility. This was calculated for each measurement using the fitted gas composition and assuming that the only other major species present was water vapor. Having a reasonable estimate of the contributions of the major species to the nonresonant susceptibility allows quantitative absolute measurements of N_2 and O_2 mole fractions.

The library of theoretical CARS spectra contains temperature intervals of 200 K between 200 and 3000 K, and between 10 and 12 values of mole fraction, depending upon the species. Oxygen mole fractions are included between 0 and 0.4, whereas the N_2 and H_2 mole fractions vary between 0 and 1. Mole-fraction values are more closely spaced near zero, to achieve better resolution at low molar concentrations. Even this coarse grid of computed spectra required 60 h to generate on a Digital Equipment Corporation alpha having a clock speed of 2.4 GHz, with a different database required for each day's runs due to variations in the instrument function from one day to the next. An initial guess of temperature and composition is obtained by comparing each measured spectrum to every theoretical spectrum in this coarse library to find a best fit. A more precise estimate of temperature and composition is then obtained using "theoretical" spectra linearly interpolated between the library entries: the absolute deviation between these theoretical spectra and the measured spectrum was minimized using a nonlinear least-squares method. Errors caused by this interpolation scheme were far smaller than other random errors in the experimental data: a set of 13 test spectra generated by CARSFIT over the expected temperature and mole-fraction ranges for this experiment were fitted with average temperature errors of 2.1 K and mole-fraction errors of less than 0.003. The largest systematic errors in fitted temperature and mole fraction for this test data were 20 K and 0.008, respectively. The fitted CARSFIT-generated spectra were convolved with instrument functions of similar width to those in the laminar flat-flame experiments, to simulate as accurately as possible the ability of the least-squares fitting routine to fit the experimental data [20]. Both these values are significantly smaller than the uncertainties in the measurements for the laminar flat-flame experiments described subsequently.

Response Surface Fitting

The experimental data were obtained using a formal experiment design method, known as modern design of experiments (MDOE). This method, first applied in the analysis of planes of CARS data in [1], with more details in [28,29], is briefly summarized here. The CARS probe volume was scanned through the flowfield along horizontal and vertical lines: one scanned line per tunnel run. The order and direction of these scans was randomized to defend against systematic errors caused by factors like heating of the duct during a facility run. In addition to the scans, repeat measurements were obtained by measuring at one spatial location throughout a single facility run, to provide a qualitative determination of the uncertainty and repeatability of the measurement system and flow facility and to allow us to determine the difference between the variance in the measurements and lack of fit to the surfaces fitted to each plane of data.

After the CARS spectra were processed to determine the temperature and the mole fractions at various locations in the duct, response surfaces were fitted to these data, providing quantitative maps of the mean temperature and mean mole fractions of nitrogen and oxygen in each of the planes. Using these fitted mean surfaces allowed us to compute statistics for the fluctuations in the measured parameters [1,28,29]. The difference between each measured sample and the mean, denoted by a primed quantity such as T' for temperature fluctuations and χ_i' for mole-fraction fluctuations of species i, is determined and the chosen fluctuation product, $T'T'$, for example, is calculated. The fluctuation product data are then fit to response surfaces, as described earlier, to determine surfaces of mean values of the product, such as $\langle T'T' \rangle$. In this way, for example, the temperature variance $\langle T'T' \rangle$ and the rms temperature fluctuation $(\langle T'T' \rangle)^{1/2}$ can be computed. Correlations between different

fluctuating properties in the flow, such as $\langle T'\chi'_{H2}\rangle$, can be calculated in the same way.

In addition to quantifying the fluctuations in the flow, the response surface allows us to reduce the uncertainty in the measured temperatures and mole fractions at a given location compared with determining the measurement uncertainty by making repeated measurements at fixed locations in the flow. This is because nearby measurements reduce the uncertainty in the measurement at the location of interest, as the surrounding data provide information about the expected value of the surface at the location of interest. This additional information is ignored if uncertainties are determined only from repeated measurements at discrete points, as that approach implicitly assumes that there is no relationship between data at different locations in the flowfield.

The functions used to determine the response surfaces depend on the spatial distribution of the data. The methodology used involves least-squares fitting most of the experimental data to a variety of surface functions and applying a series of statistical tests to determine which surface function best describes the form of the measured data. Once a surface model passes the tests, it can be tested against data that were withheld from the initial fit. The model must successfully predict the test data for a statistically significant portion of the withheld data to be considered valid. If a regression model passes all these tests, the uncertainty in the fitted surface, averaged over the surface, can be quantified as a 95% confidence-interval half width:

$$\mathrm{CIHW}_{95\%} = 2\sigma\left(\frac{p}{n}\right)^{1/2} \tag{1}$$

where σ is the fit standard error (the standard deviation of the residuals), p is the number of parameters in the surface model and n is the number of sample data points.

In the initial report of this experiment in [21] and also in the analysis of a similar data set in [20], response surface fits using the cosine series bivariate order 6 function [30] were used but were too smooth to represent the sharp gradients in temperature and species concentration present in several data maps, particularly in the shear layer between the fuel jet plume and the air. To correct for this limitation, a "saturated Gaussian" function was added to the cosine series bivariate order 6 function to better represent these steep gradients caused by injection of the fuel plume into the combustor. This function is given by

$$G_{\mathrm{sat}}(x,y) = a + b\left(1 - e^{-ce^{-\{[(x-d)/f]^2+[(y-g)/h]^2\}}}\right) \tag{2}$$

where a, b, c, d, f, g, and h are free parameters and e is the base of natural logarithms. For values of c near unity, this function resembles a positive Gaussian function. As c increases from unity, the edges of the Gaussian become steep and the top of the Gaussian becomes flat. The b parameter scales the height of the Gaussian and, when negative, represents a decrease in the measured quantity. This functional shape duplicates that observed in the experimental temperature and species mole fraction maps close to the fuel plume with better fidelity than the cosine series bivariate order 6 function alone.

It should be noted that the choice of surface fitting function is dictated by its success in passing statistical tests, rather than a judgment of whether the surface is deemed physically meaningful. These tests are expressed in terms of figures of merit that partition the variance in the data between the part of the variance that can be explained by the response surface and the unexplained variance, or divergence. The *model F-statistic* is defined as the ratio of explained variance to the unexplained variance, where the explained variance is the difference between the model and the mean value of the model averaged over all measurement locations, divided by the number of degrees of freedom in the model. The unexplained variance is the variance calculated using the measured data and the fitted surface. For this data, any fit having a model F-statistic greater than 50 passed the test [28].

The *lack-of-fit (LOF) F-statistic* is the ratio of the LOF variance to pure variance. The pure variance is determined by taking repeated measurements at a single location. The LOF variance is assumed to be the difference between the total unexplained variance and the pure variance. The *LOF P-statistic* is defined as the probability that the measured LOF F-statistic was obtained solely by chance.

As shown in Eq. (1), the confidence-interval half width increases as the square root of the number of parameters in the surface fit. For this reason, the terms in the surface fitting function with statistically insignificant coefficients are removed from the fit to minimize $\mathrm{CIHW}_{95\%}$. The significance of a coefficient is determined by whether the LOF P-statistic for that term is greater than 5% and is therefore considered by statistical fitting standards to be found by chance [31]. This removes terms that did not improve the quality of the fit, thereby improving the confidence in the remaining parameters. Removing terms removes uncertainty added by terms that did not significantly improve the fidelity of the fit. Surfaces fitted to data in this way act to smooth the data because the number of fit parameters is much smaller than the number of data points.

CARS Results

Furnace and Flame Calibrations

The CARS system was characterized by making measurements in an atmospheric-pressure furnace and a Hencken flat-flame burner [26]. Mean values of temperature and mole fraction were obtained. Mean temperature measurements in a furnace containing air in approximately 250-K increments between 300 and 1800 K agreed with thermocouple measurements within 26 K on average, whereas the mean measured mole fractions of N_2 and O_2 agreed to within 1.6% of their nominal values for atmospheric air. The temperature measurement standard deviation averaged 64 K whereas the standard deviation of the species mole fractions averaged 7.8% of the measured value for O_2 and 3.8% of the measured value for N_2, based on 200 single-shot measurements at each of the seven measured temperatures.

The measurements in a Hencken burner, which produced an atmospheric-pressure, adiabatic, H_2-air laminar, flat flame at fuel-lean and fuel-rich conditions, are summarized in Fig. 2. Results are compared to an equilibrium, adiabatic flame calculation, and the bars on the plots indicate the standard deviation of 200 measurements. Temperatures in the flame were measured with a standard deviation of ~70 K over the entire temperature range. The 95% confidence-interval half width (CIHW) uncertainty was ~10 K. The average absolute value of the difference between measured and calculated mean temperatures was 29 K, indicating systematic error sources. Mole fractions of N_2 and O_2 were measured with a standard deviation of 0.027 and 0.026, respectively, and the average absolute differences between the measurement and the calculation were 0.010 and 0.009. Errors in mole fractions were greater than expected based on random error. The standard deviation of the H_2 mole-fraction measurements in the Hencken burner varied from 0.003 at the fuel-lean equivalence ratios to a maximum of 0.028 at the maximum equivalence ratio of 3.71.

Measured H_2 mole fractions in the flat flame were systematically low by 10–15% when compared to the computation. In [21], the measured H_2 mole fraction also appeared to be low for the combustor data. Analysis of the combustor data, based upon the measured values of O_2 and N_2 mole fraction, indicates that the discrepancy is not constant, either with H_2 mole fraction or from one day's runs to the next. These errors may be either a result of inadequate spectral modeling or a systematic error in the measurement of the H_2 signal. Because of the unresolved error in the H_2 mole-fraction measurements, H_2 measurements in the combustor are not reported in this paper. Although the exact value of the fitted H_2 mole fraction is questionable, the combustor measurements produced qualitative variations in H_2 mole fraction that were consistent with expectations: the H_2 mole fractions increased as the mixture became more fuel-rich. As mentioned previously, the measured H_2 mole fraction was used to calculate the mole fraction of H_2O, which determines the nonresonant susceptibility of the mixture for each measurement. The systematic error in H_2 mole fraction can be expected to have a secondary effect on the measured values of N_2 and O_2 mole fraction.

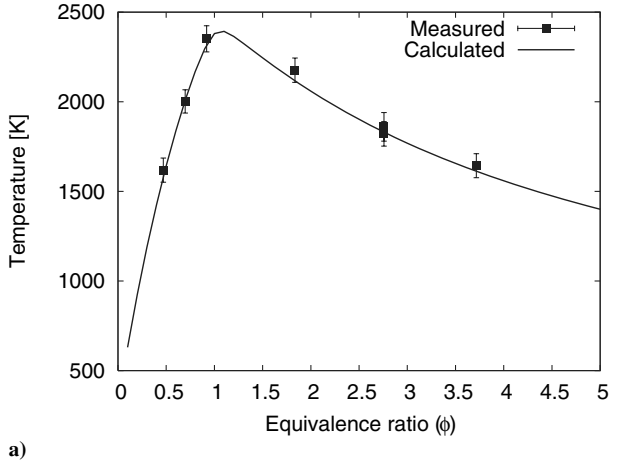

a)

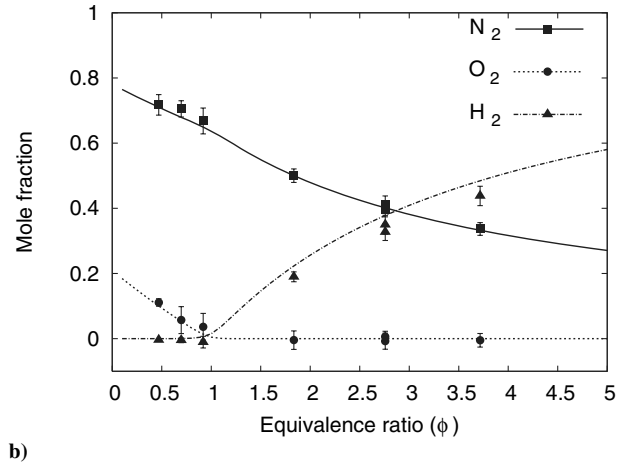

b)

Fig. 2 Hencken burner CARS calibration measurements of a) temperature and b) mole fractions of O_2, N_2, and H_2. Bars on the plots indicate the standard deviation.

Combustor Measurements

Figure 3 shows several representative CARS spectra and fits measured in the combustor. These spectra show the quality of fits to the data for planes 5 and 6, at a variety of flow conditions characteristic of the freestream conditions (3a), hot flow containing H_2 and N_2 (3b), cooler flow outside the duct in the window space (3c), and cooler flow in the unburned fuel jet plume containing only small proportions of N_2 and O_2 (3d). It should be noted that despite the relatively large interaction region, there were no measurements having an obvious dual-temperature fit caused by spatial averaging of a large temperature gradient across the interaction region. This reduces the likelihood of large temperature gradients across the interaction region, although the analysis by Zhu and Dunn-Rankin [32] shows that reasonable single-temperature fits can be generated in regions containing significant temperature gradients.

Figure 4 contains a set of measurements for a single tunnel run in which the CARS measurement volume was scanned horizontally across the duct at plane 6 at a fixed height. The coordinate system is chosen such that its origin is in the center of the duct in the freestream plane, with the bottom wall of the duct at $y = -19.8$ mm. This plot was obtained at $y = 13.7$ mm, near the center of the fuel jet plume. The plot shows the scatter of the temperature and mole fraction measurements during the scan. Most of this scatter, particularly in the high-temperature portion of the plot, is due to turbulent variations in the conditions rather than measurement random error: the boxes in Fig. 4 indicate ± 1 standard deviation at $z = -17$ mm over 200 sequential measured spectra from a tunnel run. The standard deviation of the CARS system is significantly smaller than the standard deviations in both the traverses and the repeated measurements. The cosine bivariate curve fit in Fig. 4a does not fit the large temperature gradient perfectly near the duct wall, but adequately fits the mole-fraction variations and the temperature in the middle of the duct. This poor fit near the duct wall is caused by the inability of this fitting function to capture steep gradients in the data set. Other functional forms were able to fit this steep data better near the wall, but this functional form was used because it is well-behaved in regions of the flow where there are no data and for consistency with all the other data planes.

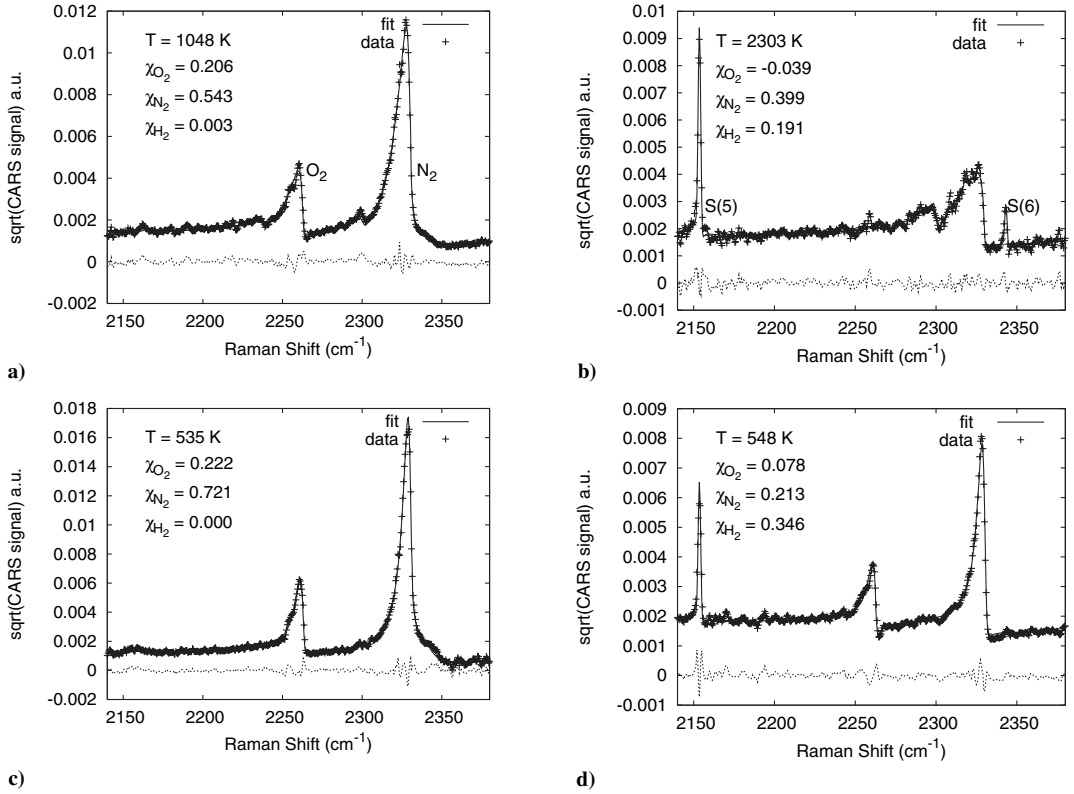

Fig. 3 Sample CARS spectra from planes 5 and 6.

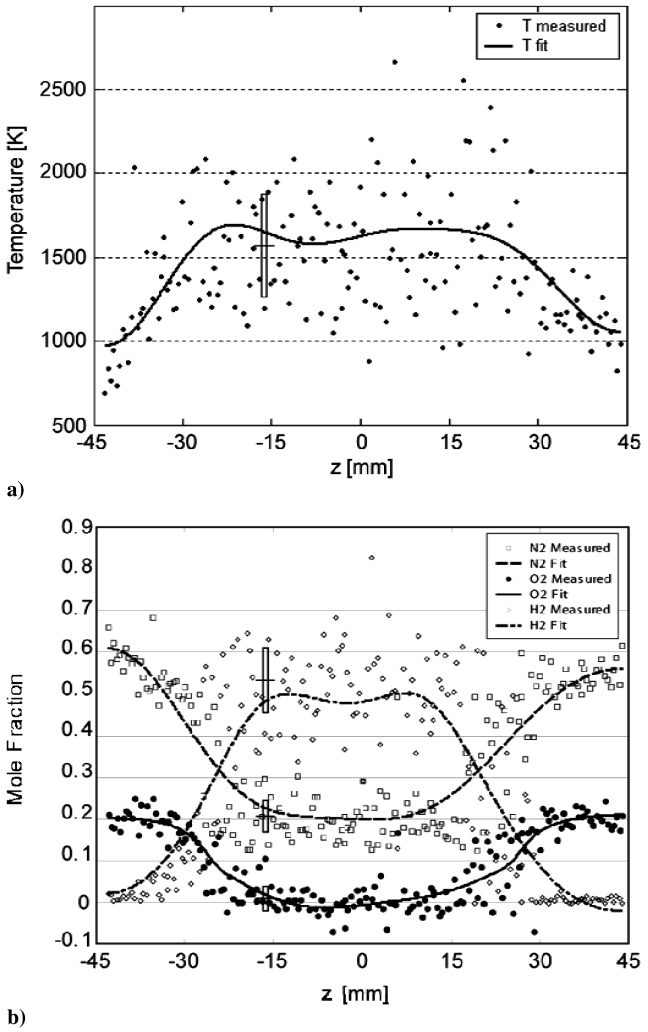

Fig. 4 a) Temperature and b) mole-fraction plots for a single facility run in plane 6. Rectangles represent mean values and standard deviations for repeated measurements at $z = -17$ mm.

The measurement locations for each of the data points are shown in Fig. 5. Each plane of data produced 2000–3000 data points, depending upon the amount of time available for runs. Most measurement planes were obtained in a single day. Plane 7 required two days of tunnel runs to generate all the necessary data. The grids indicate horizontal and vertical traverses across the duct, whereas single points away from these grid lines indicate runs for which the measurement volume was not moved during the run. Several planes also contain repeat runs along a given line, performed to test the repeatability of the measurements for nominally identical conditions.

Figure 6 is a summary of the distributions of mean temperature and species concentration, measured by the CARS system and fitted with the response surfaces. At plane 1 the mean properties are essentially uniform; the temperature might be expected to change within the boundary layers, but these are not resolved by the measurements. Taking the average of all measurements across the duct between $z = \pm 40$ mm, the measured properties are $T = 1250$ K, $\chi_{O2} = 0.204$, and $\chi_{N2} = 0.494$ with standard deviations of 151 K, 0.024, and 0.042, respectively. As previously stated, the nozzle exit conditions were calculated to be $T = 1181 \pm 60$ K, $\chi_{O2} = 0.186$, and $\chi_{N2} = 0.512$. The measurements of temperature at plane 1 do overlap with the predicted value to within the CIHW of 25 K. The fact that the temperature standard deviation is more than twice the 70 K measured in the laminar flame indicates that the temporal variations in freestream temperature are large enough to be resolved by the CARS system and that there is substantial freestream turbulence. If we assume that the real temperature fluctuations are statistically independent of the random error in the temperature

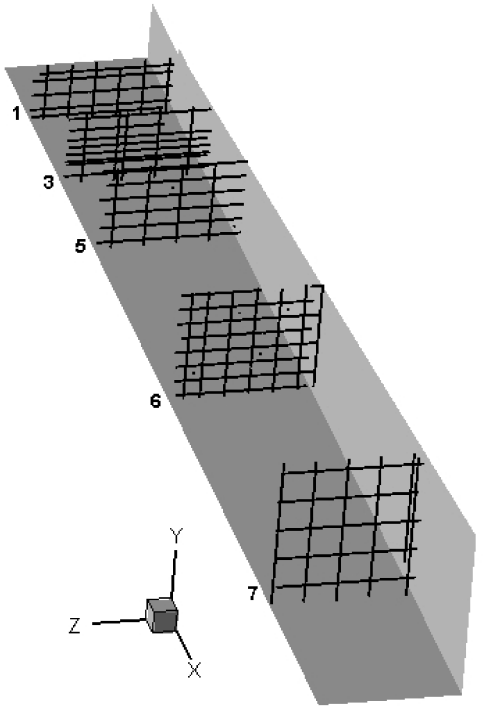

Fig. 5 Cut-away view of data acquisition locations.

measurement, and hence add in quadrature, we estimate that the standard deviation of the plane 1 temperature (the rms turbulent fluctuation level) is ~130 K. The discrepancies between the measurements of mean mole fraction and the calculations are similar in magnitude to the discrepancies between the measurements and calculations observed in the furnace and Hencken burner.

The temporal variation in the vitiated air flow away from the fuel jet was determined at plane 5 by placing the measurement volume at a fixed location (−42 mm, −6.8 mm) over 200 spectrum acquisitions. This location was away from both the fuel jet plume and the combustor wall. The mean flowfield properties over this run are $T = 944$ K, $\chi_{O2} = 0.199$, and $\chi_{N2} = 0.538$ with standard deviations of 114 K, 0.022, and 0.037, respectively. As expected, the freestream temperature in plane 5 is less than that of plane 1 because the freestream expands as the duct diverges downstream of injection. The standard deviations in temperature and mole fraction, expressed as a percentage of the mean value, are similar for both planes 1 and 5.

Another interesting outcome of the plane 1 measurements is the nonuniform distribution of both O_2 and, to a lesser extent on a percentage basis, N_2 mole fraction, with increasing concentrations of both going from left to right across the plane. This observation was consistent over two independent measurements in plane 1, and was also observed at different combustor entrance conditions in the experiments of Tedder et al. [33]. This is not an artifact of the heating of the facility during each run, because care was taken to traverse the duct in both positive and negative z directions to prevent such systematic errors. Similar asymmetries can also be seen near the edges of planes 5, 6, and 7, with the O_2 mole fraction always increasing from left to right. The systematic gradient in plane 1 O_2 concentration across the duct is approximately 0.03, greater than the average error in O_2 mole fraction for the flat-flame measurements (which was 0.01). The plane 1 temperature map does not show an obvious gradient. These trends do not appear to be self-consistent (a composition variation would predict a temperature variation) nor consistent with the way the facility heater is constructed (axisymmetric); this discrepancy remains unresolved.

The temperature maps in Fig. 6 can be directly compared with the previous conventional broadband N_2 CARS measurements [1] obtained at the same nominal conditions. Upon comparing the temperature surface fits for the two campaigns, the temperatures averaged over the plane were found to differ by −97, −6, −95, 90, and −17 K in planes 1, 3, 5, 6, and 7, respectively. The greatest

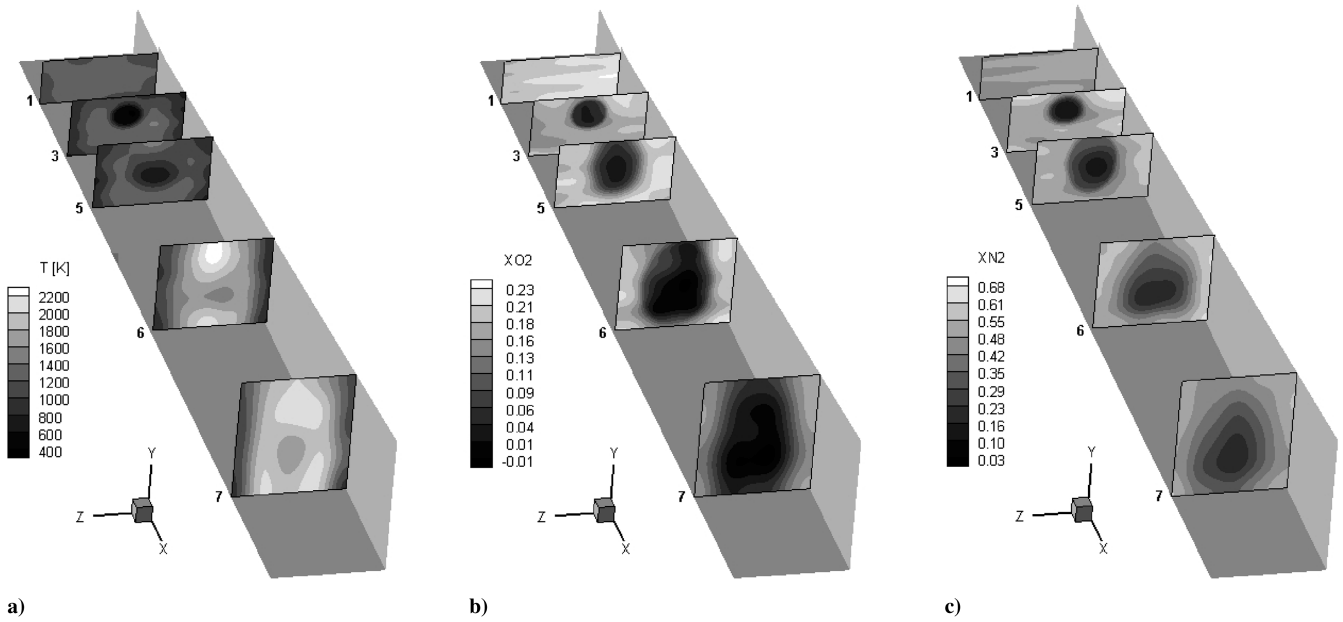

Fig. 6 Maps of a) mean temperature, b) mean O_2 mole fraction, and c) mean N_2 mole fraction.

difference between the surface fits occurred in plane 1. The plane 1 average temperature in [1] is 1162 K, with CIHW of 30 K, whereas the average in plane 1 for the current series of experiments is 1250 K. More detailed comparisons show a systematic difference of 80–120 K throughout the central part of the combustor, with the dual-pump CARS producing the higher temperatures.

Initially it was thought that a possible reason for the discrepancy between the conventional and dual-pump CARS measurements in plane 1 was due to a leak in the nozzle cooling water system that developed during acquisition of the dual-pump CARS data, causing cooling water to enter the flow. Some preliminary dual-pump CARS measurements had been performed in plane 1 before the leak had been detected, allowing us to compare these two data sets to see if the average temperature had changed after the repair. The preliminary measurements were performed at the very beginning of the dual-pump CARS experimental campaign, when the combustor was configured exactly as it had been in the experiments of [1]. Figure 7 compares two horizontal traverses at $y = -1.8$ mm: one obtained before the nozzle repair and another obtained afterwards and used for the plane 1 surface presented in Fig. 6. This plot plainly shows little difference between the measured temperatures for the two traverses. The plane-averaged temperatures agree to within 27 K, or 2.1%, of one another. The agreement is similarly good for other traverses in the same region, and between the N_2 and O_2 mole-fraction measurements in the two plane 1 dual-pump CARS experiments. One difference between the two measurements in Fig. 7 is that the

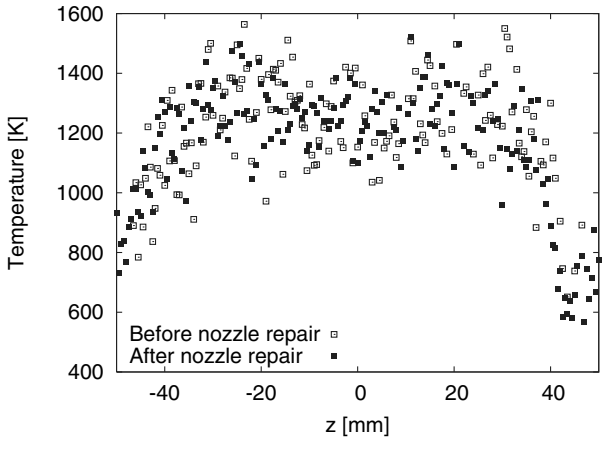

Fig. 7 Data for facility runs obtained before and after nozzle repair.

110-K standard deviation of the second series of measurements is noticeably smaller than the 140-K standard deviation in the first plane 1 measurement. This difference is due to a reduction in instrument random error derived from the ability to remotely align two of the pump beams between experiments (thereby increasing signal level). This capability was added in the period between the two measurements. Considering that the temperature measurements in Fig. 7 were obtained two months apart, with data for planes 3, 5, 6, and 7 acquired between the two measurements, the dual-pump CARS measurements and the facility combustor entrance flow are consistent.

The reasons for the discrepancy between the dual-pump CARS temperature measurements and those of [1] for plane 1 are not known. The good agreement between the dual-pump measurements in the Hencken burner and adiabatic flame calculations, and a greater confidence in the spectral fitting process due to the presence of O_2 spectra as well as N_2 in our measurements, gives us more confidence in the plane 1 dual-pump CARS measurements than for the single-pump CARS measurements.

Returning to Fig. 6, the first strong indications of combustion occur at the top of the duct in plane 5, where the temperature increases to a peak value of approximately 1600–1700 K, compared to 800–900 K for the same location in a previous mixing-only experiment [26]. This also corresponds to a region of reduction of the O_2-to-N_2 ratio above the center of the fuel plume, indicating consumption of O_2 by combustion. The fact that combustion is already occurring in plane 5 is of interest, because there was some concern that the flow was igniting at the interface between the copper and stainless steel ducts, indicating that this junction may have been strongly influencing flame holding in the combustor. The plane 5 measurements indicate that the flow is autoigniting upstream of the junction.

The plane 5 mole fraction plots show that, at this location, the fuel jet plume's edge has penetrated nearly to the lower duct wall, as shown by the deficit in N_2 mole fraction near the bottom wall. In the initial analysis of this plane 5 data an unexpected bifurcation of the plume was observed in the O_2 and N_2 distributions [21]. Upon closer inspection, this was caused by including in the data an incorrect y value for one of the scans. By correcting this error in accordance with the original data logbook, the expected round plume was obtained, as seen in the figure.

At plane 6, some fuel products have penetrated to the bottom of the duct, distorting the plume near the duct floor. The minimum value of N_2 is higher than for the previous planes, as would be expected from a flow that is becoming better mixed as it flows along the duct. The

Table 1 Statistical 95% confidence-interval half-width uncertainties (CIHW) in fitted surfaces, and results of the model F-statistic (Mod F) and lack-of-fit P-statistic (LOF P) tests

Parameter	Plane 1			Plane 3			Plane 5			Plane 6			Plane 7		
	CIHW	Mod F	LOF P	CIHW	Mod F	LOF P	CIHW	Mod F	LOF P	CIHW	Mod F	LOF P	CIHW	Mod F	LOF P
$\langle T \rangle$	25	P	F	36	P	P	50	P	P	41	P	P	40	P	P
$\langle \chi_{N2} \rangle$	0.0058	P	P	0.017	P	P	0.016	P	F	0.012	P	P	0.010	P	P
$\langle \chi_{O2} \rangle$	0.0034	P	P	0.0073	P	P	0.0084	P	P	0.0094	P	F	0.0068	P	P
$\langle T'T' \rangle$	4600	F	F	9900	P	P	18000	P	P	15000	P	P	12000	F	P
$\langle \chi'_{N2}\chi'_{N2} \rangle$	0.00035	F	P	0.0025	P	P	0.0020	P	F	0.0014	P	P	0.00070	P	P
$\langle \chi'_{O2}\chi'_{O2} \rangle$	0.000053	F	P	0.00067	F	F	0.00051	P	P	0.00070	P	F	0.00043	P	F
$\langle T'\chi'_{N2} \rangle$	0.81	F	F	4.4	P	P	3.4	P	P	4.1	P	P	2.7	P	P
$\langle T'\chi'_{O2} \rangle$	0.32	F	P	1.6	P	P	1.9	P	P	1.8	P	P	1.7	P	F
$\langle \chi'_{N2}\chi'_{O2} \rangle$	0.00011	F	P	0.00091	P	P	0.00091	P	F	0.00066	P	P	0.00033	P	F

region of reduced O_2 mole fraction corresponds to the region of highest temperature in the temperature map. This supports the view that combustion is strongest in that region of the flow.

Plane 7 looks more symmetrical left to right than planes 5 and 6, where the fuel jet plume is shifted slightly towards the right of the duct. The difference is particularly noticeable in the temperature distribution. The aforementioned repair to the nozzle required both the copper and steel sections of the combustor to be removed. Plane 7 properties were measured after the model was reassembled, whereas planes 3, 5, and 6 (and the data of [1]) were measured before this; it is likely that the duct sections were better aligned for plane 7 than for the previous tests, resulting in a more symmetric distribution. This is consistent with the results of [1], which were slightly asymmetrical at planes 5, 6, and 7.

Table 1 summarizes the uncertainty in the fits for these mean quantities. These values represent the 95% CIHW uncertainty in the fit's prediction of the mean surface, averaged over the entire surface of a given plane. For these mean property maps, the statistical uncertainties are typically nearly twice the systematic errors discovered during the flame and furnace calibration studies. For example, typical temperature measurement fit uncertainties were 25–50 K, whereas systematic errors were on the order of 30 K. Similarly, the statistical fit uncertainties for N_2 and O_2 mole fraction were between 0.003 and 0.017, whereas the systematic errors were less than or equal to 0.01. These results indicate that acquiring a factor of 2 or more data per plane (reducing these statistical uncertainties by a factor of 1.4) would have been a sensible investment of resources. However, acquiring more than four times more data would reduce the statistical errors to a level lower than the systematic errors, which would probably be a poor use of resources.

Table 1 also shows whether each fitted surface passed or failed the model F-statistic and lack-of-fit (LOF) P-statistic tests as described in [28,29]. Failure of the model F-statistic test indicates poor signal-to-noise ratio in the surface being fitted. All 15 of the mean surface fits passed the model F-statistic test, indicating good signal-to-noise in the fits. Failure to exceed a LOF P-statistic of 0.05 indicates that a fit may contain significant lack of fit: that is, the response surface may be a poor fit to the data. Three of the 15 mean surfaces fitted failed this LOF P-statistic test. Truncating steep gradients at the edge of the data domain and refitting resulted in a passed LOF P-statistic. Alternately, choosing other functional forms produced slightly better fits that pass this test, in some cases. However, this was not done because it was more consistent to use the same basis functions for all of the surfaces, to avoid introducing another variable into the analysis. Because these statistics depend on the overall quantity of data obtained, it is possible that taking a factor of 2 or more data would have resulted in fits that passed the LOF P-statistic test.

Spatial Variation in Fluctuating Parameters

As mentioned in the introduction, one of the main benefits of dual-pump CARS as a measurement technique is that it allows more than one flow property to be measured simultaneously. This capability allows us to determine statistical correlations between each of the measured flow properties in the duct. Such information is useful in the development of turbulence models for CFD simulations, and also provides important information about mixing in this particular combustor.

We classify the correlations into three categories: variances, such as $\langle T'T' \rangle$, $\langle \chi'_{O2}\chi'_{O2} \rangle$, and $\langle \chi'_{N2}\chi'_{N2} \rangle$; covariances between the various mole fractions, such as $\langle \chi'_{N2}\chi'_{O2} \rangle$; and covariances between the temperature and various mole fractions, such as $\langle T'\chi'_{N2} \rangle$ and $\langle T'\chi'_{O2} \rangle$. Surfaces of the square root of the variances and covariances are presented in Figs. 8 and 9. Each of these plots has regions of low fluctuation at the edges of the plot, where the gas is mostly freestream, and in the center of the plot, where much of the flow is H_2 from the fuel jet. Between these two regions, all four maps show regions of large fluctuations, particularly along the sides of the fuel plume. The shear between the plume and the freestream generates large fluctuations in both temperature and species concentration.

Compare the plane 7 $\langle T'T' \rangle$ map shown in Fig. 8a with the mean temperature map shown in Fig. 6. The $\langle T'T' \rangle$ map shows large temperature fluctuations near the bottom of the duct (approximately 460 K) but much smaller fluctuations at the top (approximately 250 K). The mean temperature distribution contains peaks at the top and bottom portions of the duct. This combination indicates that turbulent mixing and combustion are still taking place at the bottom of the duct as evidenced by large temperature fluctuations, but the hot flow at the top of the duct has become more evenly mixed and burnt. This result is consistent with observations made in [1].

Consider the temperature/mole-fraction covariance maps, summarized in Fig. 9. At plane 3, the $\langle T'\chi'_{N2} \rangle$ and $\langle T'\chi'_{O2} \rangle$ maps show strong positive correlations at the center of the fuel jet plume, meaning that high temperatures correspond to high mole fraction of N_2 and O_2 and vice versa. Recall that the fuel is injected at a temperature well below the freestream temperature, so that instantaneously low measured temperatures correspond to instantaneously high mole fraction of H_2 and low mole fraction of the remaining species. Elsewhere in plane 3, the correlations are approximately zero. For the most part, the $\langle T'\chi'_{O2} \rangle$ and $\langle T'\chi'_{N2} \rangle$ covariance maps are similar to each other. However, for planes 6 and 7, the $\langle T'\chi'_{O2} \rangle$ covariance map shows some regions of significant negative correlation. This means that in these regions the instantaneously hotter-than-average gas has lower-than average O_2 content. Presumably, higher temperature coincides with more combustion, and more consumed O_2. The regions of large positive correlation at the bottom of the duct may, using the same argument, indicate that the instantaneous concentration of O_2 is controlled by the process of mixing with air rather than by combustion. Many of the insights drawn from these plots are common sense, but the value of the plots lies in knowing the magnitude and the location in the duct where these fluctuations occur.

Figure 9c contains the mole-fraction covariance maps for $\langle \chi'_{N2}\chi'_{O2} \rangle$. In planes 5 and 6, large positive correlations between N_2 and O_2 clearly identify the mixing layer around the fuel jet plume. However, at the center of the plume N_2 and O_2 are uncorrelated. This is sensible, because the bulk of O_2 that has diffused to the center of the fuel jet plume would have combusted.

Danehy et al. [29] showed that many more measurements are required to measure rms fluctuations of properties with an acceptable

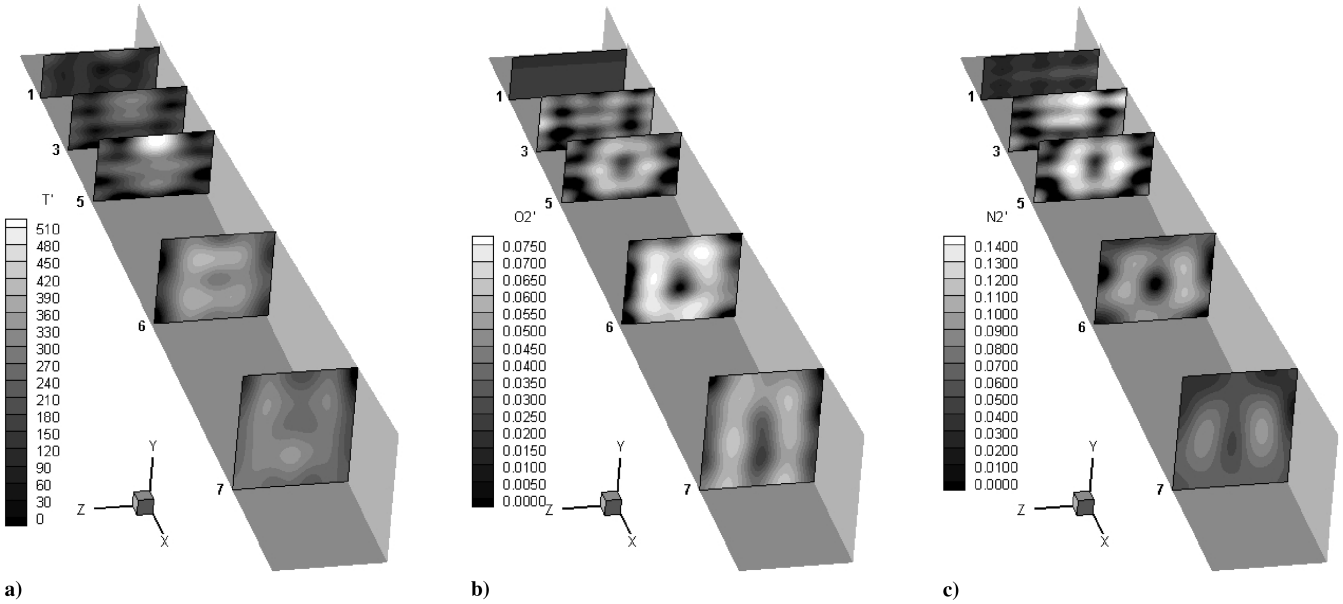

Fig. 8 Maps of square root of variance: a) $(\langle T'T' \rangle)^{1/2}$, b) $(\langle \chi'_{O2}\chi'_{O2} \rangle)^{1/2}$, and c) $(\langle \chi'_{N2}\chi'_{N2} \rangle)^{1/2}$.

uncertainty than are required to measure the means of these properties. The uncertainties of the fits to these fluctuating parameters are also presented in Table 1, in which they are once again averaged over the entire plane. On a percentage basis, CIHW values for these measurements varied from 10 to 15% of the maximum fitted values, averaged over the entire plane. Some of the fits fail the model F-statistic and lack-of-Fit P-statistic tests. These tests could probably be passed if more data of the same quality were obtained (both statistics improve with larger data volume). The data are included as proof that such measurements can be made with the current system, although more measurements would be required to reduce the uncertainty to levels that would be acceptable for CFD model development and validation. In their present form the measurements of fluctuation in this data are sufficient to indicate the regions in the flow where interesting fluctuations in flow properties occur.

Table 1 also shows that just under half of the fluctuation maps shown in Figs. 8 and 9 pass the model F-statistic test, indicating that the signal-to-noise ratio in the data is too low to allow a good fit. Those that failed the fit only failed by a factor of 2, indicating that, if twice as much data had been obtained, they probably would have passed the test. The fact that these fits failed the tests means that there are probably small amplitude variations shown in the graphs that are not real: rather, they are fitting to noise. Nonetheless, the larger features shown in the maps are real. Furthermore, a few of the surface fits failed the lack-of-fit P-statistic test. As stated earlier, choosing different fit functions can result in satisfactory fits, but we did not do so, to avoid introducing another variable into the analysis.

Conclusions

We have used the dual-pump CARS measurement technique to simultaneously measure temperature and the absolute mole fractions of O_2 and N_2 in a model supersonic combustor. Nearly 12,000 single-shot measurements were obtained in five different measurement planes oriented perpendicular to the flow direction. These measurements were fitted with analytic surfaces to provide 2-D maps of each mean flow property in each of the five planes. The maps were used, together with the raw data, to compute fluctuating quantities and their correlations, including $\langle T'T' \rangle$, $\langle T'\chi'_{N2} \rangle$, and $\langle \chi'_{O2}\chi'_{N2} \rangle$, among others. This type of data should be useful for

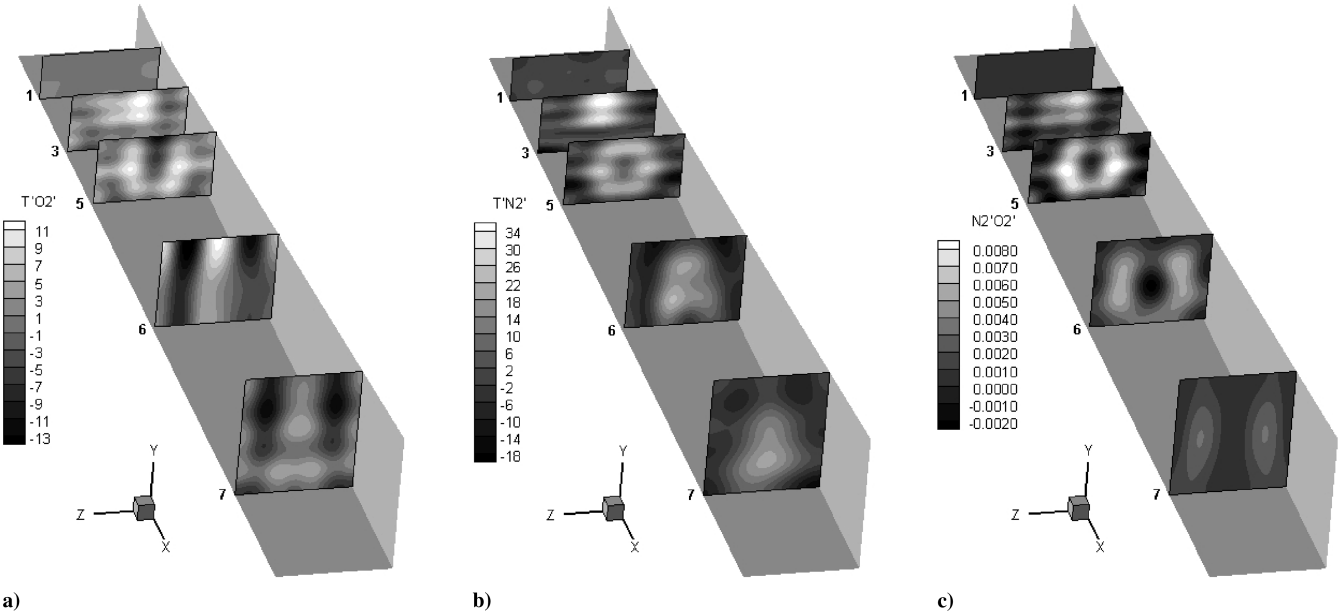

Fig. 9 Maps of temperature/mole-fraction covariances: a) $\langle T'\chi'_{O2} \rangle$, b) $\langle T'\chi'_{N2} \rangle$, c) $\langle \chi'_{N2}\chi'_{O2} \rangle$.

developing new models to predict turbulent flow, mixing, and combustion.

The standard deviation of the temperature measurement technique, as determined in flame and furnace calibration experiments, is less than the standard deviation of the freestream temperature, allowing an estimate of the upper limit of facility flow temperature fluctuations to be made. These measurements indicate that standard deviations in the freestream temperature at the facility nozzle exit were ~130 K. Nozzle exit fluctuations in mole fraction were of the same order as the fluctuations measured in a premixed laminar flat flame, and were therefore not resolved by the technique. Upper limits for standard deviations of 0.024 and 0.042 were measured for O_2 and N_2, respectively.

The data presented here show combustion being strongest at the top and bottom of the duct, spreading towards the sides of the duct as the flow proceeds downstream. Examination of the intensity of fluctuations about the mean allows us to determine where significant mixing and combustion are occurring in the flowfield.

The CARS system, analysis, and application described in this paper could be improved in several ways. First, the observed errors in H_2 mole fraction should be investigated so that the H_2 data obtained in the combustor can be analyzed and presented to complement the work outlined in the current paper. Measurements in a high-temperature static cell using several known H_2 concentrations at different temperatures would provide the necessary controlled environment for characterizing the systematic error. Second, the combination of an injection-seeded YAG laser and modeless dye laser may improve the precision of the measurements. Third, more data would reduce measurement uncertainty. This could be achieved in the same amount of facility time using a pump laser with a higher repetition rate. In future work, an axisymmetric flowfield will be investigated, as the assumption of symmetry allows more precise determination of flow properties and their correlations with data sets of comparable size. Furthermore, a velocity measurement technique will be developed that operates simultaneously with the CARS method to provide much-needed mean velocity profiles as well as correlations between velocities, temperatures, and mole fractions.

Acknowledgments

We wish to acknowledge the assistance of Diego Capriotti from NASA Langley Research Center for coordinating the running of the facility and processing of facility data for this paper. We also thank Jeff White, for assisting us in computing libraries of CARS spectra on a large cluster of personal computers, significantly decreasing the computational time. In addition, we thank Robert Lucht from Purdue University for suggestions and discussion of CARS spectral modeling issues.

References

[1] Cutler, A. D., Danehy, P. M., Springer, R. R., O'Byrne, S., Capriotti, D. P., and DeLoach, R., "Coherent Anti-Stokes Raman Spectroscopic Thermometry in a Supersonic Combustor," *AIAA Journal*, Vol. 41, No. 12, Dec. 2003, pp. 2451–2459.

[2] Smith, M. W., Jarratt, O., Jr., Antcliffe, R. R., Northam, G. B., Cutler, A. D., and Taylor, D. J., "Coherent Anti-Stokes Raman Spectroscopy Temperature Measurements in a Hydrogen-Fueled Supersonic Combustor," *Journal of Propulsion and Power*, Vol. 9, No. 2, 1993, pp. 163–168.

[3] Yang, S. R., Zhau, J. R., Sung, G. J., and Yu, G., "Multiplex CARS Measurements in Supersonic Hydrogen/Air Combustion," *Applied Physics B, Lasers and Optics*, Vol. 68, No. 2, 1999, pp. 257–265.

[4] Grisch, F., Bouchardy, P., and Clauss, W., "CARS Thermometry in High Pressure Rocket Combustors," *Aerospace Science and Technology*, Vol. 7, No. 4, 2003, pp. 317–330.

[5] Anderson, T. J., and Eckbreth, A. C., "Simultaneous Coherent Anti-Stokes Raman Spectroscopy Measurements in Hydrogen-Fueled Supersonic Combustion," *Journal of Propulsion and Power*, Vol. 8, No. 1, 1992, pp. 7–15.

[6] Weisgerber, H., Fischer, M., Magens, E., Winandy, A., Foerster, W., and Beversdorff, M., "Experimental Analysis of the Flow of Exhaust Gas in a Hypersonic Nozzle," AIAA Paper 98-1600, April 1998.

[7] Vereschagin, K. A., Smirnov, V. V., Stelmakh, O. M., Fabelinski, V. I., Sabelnikov, V. A., Ivanov, V. V., Clauss, W., and Oschwald, M., "Temperature Measurements by Coherent Anti-Stokes Raman Spectroscopy in Hydrogen-Fuelled Scramjet Combustor," *Aerospace Science and Technology*, Vol. 5, No. 5, 2001, pp. 347–355.

[8] McIntyre, T. J., Houwing, A. F. P., Palma, P. C., Rabbath, P., and Fox, J. S., "Imaging of Combustion in a Supersonic-Combustion Ramjet," *Journal of Propulsion and Power*, Vol. 13, No. 3, 1996, pp. 388–394.

[9] McMillin, B. K., Palmer, J. L., and Hanson, R. K., "Temporally Resolved 2-Line Fluorescence Imaging of NO Temperature in a Transverse Jet in a Supersonic Cross-Flow," *Applied Optics*, Vol. 32, No. 36, 1993, pp. 7532–7545.

[10] Donohue, J. M., and McDaniel, J. C., "Complete Three-Dimensional Multi-Parameter Mapping of a Supersonic Ramp Injector Flowfield," *AIAA Journal*, Vol. 34, No. 3, 1996, pp. 455–466.

[11] Laufer, G., Quagliaroli, T. M., Krauss, R. H., Whitehurst, R. B., and McDaniel, J. C., "Planar OH Density and Apparent Temperature Measurements in a Supersonic Combusting Flow," *AIAA Journal*, Vol. 34, No. 3, 1996, pp. 463–469.

[12] Eckbreth, A. C., *Laser Diagnostics for Combustion, Temperature and Species*, Abacus Press, Kent, U.K., 1996.

[13] Antcliff, R. R., and Jarrett, O., Jr., "Multispecies Coherent Anti-Stokes Raman Scattering Instrument for Turbulent Combustion," *Review of Scientific Instruments*, Vol. 58, No. 11, 1987, pp. 2075–2080.

[14] Boyack, K., and Hedman, P. O., "Dual-Stokes CARS System for Simultaneous Measurement of Temperature and Multiple Species in Flames," *Proceedings of the Twenty-Third Symposium (International) on Combustion*, The Combustion Institute, Pittsburgh, PA, 1990, pp. 1893–1899.

[15] Schenk, M., Thumann, A., Seeger, T., and Liepertz, A., "Pure Rotational Coherent Anti-Stokes Raman Scattering Comparison of Evaluation Techniques for Single-Shot Temperature and Relative N_2-O_2 Concentration Determination," *Applied Optics*, Vol. 37, No. 24, 1998, pp. 5659–5671.

[16] Schenk, M., Seeger, T., and Leipertz, A., "Simultaneous Temperature and Relative O_2-N_2 Concentration Measurements by Single-Shot Pure Rotational Coherent Anti-Stokes Raman Scattering for Pressures as Great as 5 MPa," *Applied Optics*, Vol. 39, No. 26, 2000, pp. 6918–6925.

[17] Aldén, M., Bengtsson, P., Edner, H., Kröll, S., and Nilsson, D., "Rotational CARS: a Comparison of Different Techniques with Emphasis on Accuracy in Temperature Determination," *Applied Optics*, Vol. 26, No. 15, 1989, pp. 3206–3219.

[18] Lucht, R. P., "Three-Laser Coherent Anti-Stokes Raman Scattering Measurements of Two Species," *Optics Letters*, Vol. 12, No. 2, Feb. 1987, pp. 78–80.

[19] Hancock, R. D., Schauer, F. R., Lucht, R. P., and Farrow, R. L., "Dual-Pump Coherent Anti-Stokes Raman Scattering Measurements of Nitrogen and Oxygen in a Laminar Jet Diffusion Flame," *Applied Optics*, Vol. 36, No. 15, 1997, pp. 3217–3226.

[20] Danehy, P. M., O'Byrne, S., Cutler, A. D., and Rodriguez, C. G., "Coherent Anti-Stokes Raman Scattering (CARS) as a Probe for Supersonic Hydrogen-Fuel/Air Mixing," *Proceedings of the JANNAF APS/CS/PSHS/MSS Joint Meeting* [CD-ROM], CPIA, Columbia, MD, Dec. 2003.

[21] O'Byrne, S., Danehy, P. M., and Cutler, A. D., "Dual-Pump CARS Thermometry and Species Concentration Measurements in a Supersonic Combustor," AIAA Paper 2004-0710, Jan. 2004.

[22] Roy, S., Meyer, T. R., Brown, M. S., Velur, V. N., Lucht, R. P., and Gord, J. R., "Triple-Pump Coherent Anti-Stokes Raman Scattering (CARS): Temperature and Multiple-Species Concentration Measurements in Reacting Flows," *Optics Communications*, Vol. 224, No. 1, 2003, pp. 131–137.

[23] Lucht, R. P., Natarajan, V. V., Carter, C. D., Grinstead, K. D., Jr., Gord, J. R., Danehy, P. M., Fiechtner, G. J., and Farrow, R. L., "Dual-Pump Coherent Anti-Stokes Raman Scattering Temperature and CO_2 Concentration Measurements," *AIAA Journal*, Vol. 41, No. 4, April 2003, pp. 679–686.

[24] Auslender, A. H., "An Application of Distortion Analysis to Scramjet Combustor Performance Assessment," *1996 JANNAF Propulsion and Joint Subcommittee Meeting Scramjet Performance Workshop*, edited by R. S. Fry and M. F. Blackburn, CPIA, Columbia, MD, 1996.

[25] Springer, R. R., Cutler, A. D., Diskin, G. S., and Smith, M. W., "Conventional/Laser Diagnostics to Assess Flow Quality in a Combustion-Heated Facility," AIAA Paper 99-2170, June 1999.

[26] O'Byrne, S., Danehy, P. M., and Cutler, A. D., "$N_2/O_2/H_2$ Dual-Pump CARS: Validation Experiments," *20th International Congress on Instrumentation in Aerospace Simulation Facilities*, Göttingen, Germany, Aug. 2003.

[27] Palmer, R. E., "The CARSFT Computer Code for Calculating Coherent Anti-Stokes Raman Spectra: User and Programmer Information,"

Sandia National Laboratories Report SAND89-8206, Livermore, CA, 1989.
[28] Danehy, P. M., DeLoach, R., and Cutler, A. D., "Application of Modern Design of Experiments to CARS Thermometry in a Model Scramjet Engine," AIAA Paper 2002-2914, June 2002.
[29] Danehy, P. M., Dorrington, A. A., Cutler, A. D., and DeLoach, R., "Response Surface Methods for Spatially-Resolved Optical Measurement Techniques," AIAA Paper 2003-0648, Jan. 2003.
[30] TableCurve®3D User's Manual, Ver. 3.0, AISN Software, Mapleton, OR, 1997.
[31] Kraber, S., *Handbook for Experimenters*, Ver. 06.8, Stat-Ease, Minneapolis, MN, 2002, pp. 3–20.
[32] Zhu, J. Y., and Dunn-Rankin, D., "CARS Thermometry in High Temperature Gradients," *Applied Physics B, Lasers and Optics*, Vol. 56, No. 1, 1993, pp. 47–55.
[33] Tedder, S., O'Byrne, S., Danehy, P. M., and Cutler, A. D., "CARS Temperature and Species Concentration Measurements in a Supersonic Combustor with Normal Injection," AIAA Paper 2005-616, 2005.

R. Lucht
Associate Editor